ELSEVIER

Journal of Nuclear Materials 295 (2001) 249–264

journal of nuclear materials

www.elsevier.nl/locate/jnucmat

Kinetic and thermodynamic studies of the dissolution of thorium–uranium (IV) phosphate–diphosphate solid solutions

A.C. Thomas [a], N. Dacheux [a,*], P. Le Coustumer [b], V. Brandel [a], M. Genet [a]

[a] *Groupe de Radiochimie, Institut de Physique Nucléaire, IPN, Bât 100, Université de Paris Sud-XI, 91406 Orsay cedex, France*
[b] *LMGE, UMR-CNRS 6532, ESIP, 40 av. Pineau, 86022 Poitiers cedex, France*

Received 7 February 2001; accepted 1 March 2001

Abstract

The dissolution of thorium–uranium (IV) phosphate–diphosphate solid solutions (TUPD) was studied as a function of the temperature and leachate acidity. The dependence of the normalized dissolution rate on the temperature leads to an activation energy equal to about 40 kJ mol^{-1}, close to that obtained for the pure thorium phosphate–diphosphate (42 ± 3 kJ mol^{-1}) and for thorium–plutonium (IV) phosphate–diphosphate solid solutions (41 ± 1 kJ mol^{-1}). The normalized dissolution rate of TUPD slightly increases with the leachate acidity. The partial order related to the proton concentration, n, is equal to 0.40 ± 0.02 while the apparent normalized dissolution rate constant, $k'_{T,I}$, reaches $(2.8 \pm 0.7) \times 10^{-4}$ g m^{-2} d^{-1} at 90°C and for $[H_3O^+] = 1$ M. When the saturation of the leachate is reached, the concentration of thorium, uranium and phosphate ions measured in the solution are controlled by the precipitation of the uranyl phosphate pentahydrate $(UO_2)_3(PO_4)_2 \cdot 5H_2O$ and the thorium phosphate–hydrogenphosphate $Th_2(PO_4)_2(HPO_4) \cdot H_2O$. Both solids were extensively characterized using XRD, infrared and UV–visible spectroscopies or electron probe microanalysis (EPMA). Their solubility products, $K^{\circ}_{S,0}$, were determined and extrapolated to $I = 0$. They are equal to $10^{-55.2 \pm 0.5}$ and $10^{-66.6 \pm 1.2}$, respectively. All the samples leached were characterized using EPMA, SEM and TEM. These techniques showed that during the dissolution process, thorium and uranium are completely separated as $(UO_2)_3(PO_4)_2 \cdot 5H_2O$, on one hand, and $Th_2(PO_4)_2(HPO_4) \cdot H_2O$, on the other hand. In the first days of leaching tests, an amorphous additional phase, identified as $Th_2(PO_4)_2(HPO_4) \cdot nH_2O$ was also observed. Several leaching tests performed on sintered TUPD samples revealed that the dissolution rates measured in 10^{-1} M HNO_3 is very low (6.5×10^{-5} g d^{-1}) by comparison to other ceramics studied in the same objective. In these conditions, the thorium phosphate–diphosphate (TPD) appears as a promising ceramic for the immobilization of tetravalent actinides like uranium, neptunium or plutonium.

1. Introduction

Several phosphate matrices like apatite [1], monazite [2] or sodium zirconium phosphate (NZP) [3] were already proposed in the literature as potential host matrices for nuclear waste storage due to their resistance to radiation damages, aqueous corrosion and to their capability to form solid solutions with actinides. In this context, we completely re-examined the chemistry of uranium and thorium phosphates considering their properties which could be applied for the actinides immobilization [4–6]. We already reported the synthesis and the characterization of the thorium phosphate–diphosphate $Th_4(PO_4)_4P_2O_7$ (so called TPD) which is very resistant to aqueous corrosion [7]. We studied the replacement of thorium by tetravalent plutonium in the TPD structure leading to the formation of $Th_{4-x}Pu_x(PO_4)_4P_2O_7$ (TPPD) solid solutions [8–11]. Plutonium isotopes produce, by decay, several uranium isotopes like ^{238}U (daughter product of ^{242}Pu : α, $T_{1/2} = 3.75 \times 10^5$ yr), ^{236}U (daughter product of ^{240}Pu : α, $T_{1/2} = 6563$ yr), ^{235}U (daughter product of ^{239}Pu : α, $T_{1/2} = 2.4 \times 10^4$ yr) and ^{234}U (daughter prod-

* Corresponding author. Tel.: +33-1 69 15 73 42; fax: +33-1 69 15 71 50.
E-mail address: dacheux@ipno.in2p3.fr (N. Dacheux).

0022-3115/01/$ - see front matter
PII: S0022-3115(01)00534-7

uct of $^{238}Pu : \alpha, T_{1/2} = 87.74$ yr). Moreover, one of the main plutonium isotopes: ^{241}Pu ($T_{1/2} = 14.4$ yr) is β^- emitter and produces by decay americium ^{241}Am ($\alpha, T_{1/2} = 432$ yr) then finally neptunium ^{237}Np ($\alpha, T_{1/2} = 2 \times 10^6$ yr). For this reason, we were also interested in the replacement of thorium by tetravalent uranium [8–11] or neptunium [12] in the TPD structure. The conditions of preparation of $Th_{4-x}U_x(PO_4)_4P_2O_7$ (TUPD) and $Th_{4-x}Np_x(PO_4)_4P_2O_7$ (TNPD) solid solutions were already extensively reported in several of our published works [6–12]. Moreover, TUPD solid solutions were prepared as sintered pellets after a room-temperature pressing at 200–800 MPa then heating treatment at 1250°C for 10–30 h. In these conditions, the density of the pellets reached 95–99% of the value calculated from XRD data [13,14].

The use of material for the nuclear waste storage is often based on its capability to resist to aqueous corrosion. For this reason, we performed a systematic study of the dissolution of the pure TPD from a kinetic point of view (dependence of the normalized dissolution rate on several parameters such as temperature, acidity of the leachate, phosphate concentration,...) on one hand, and from a thermodynamic point of view (i.e. identification of neoformed phases precipitated in the back-end of the TPD dissolution) on the other hand. The same study was developed for thorium–uranium (IV) phosphate–diphosphate (TUPD) solid solutions by making several leaching tests on the solids synthesized. We studied the release of uranium in the solution in order to determine the normalized leaching (or dissolution) rate. Because of the very low dissolution rate of the TPD, and in order to put in evidence the phases neoformed when the saturation of the leachate is reached, we also increased the dissolution process by making the experiments in several acidic media at 90°C.

The present study deals with the influence of the temperature and acidity of the leachate on the normalized dissolution rate and the analysis of the neoformed phosphate phases which control the concentration of uranium, thorium and phosphate in the leachate when the saturation of the solution is reached.

2. Experimental

2.1. Chemicals and apparatus

Uranium (IV) chloride solution ($C_U = 1.1$–1.5 M) was prepared by dissolving uranium metal chips in concentrated hydrochloric acid. The thorium chloride solution was prepared by dilution of a concentrated solution ($C_{Th} = 1.8$ M) provided by Rhone–Poulenc. All the other chemicals used (phosphoric, perchloric or nitric acids, sodium perchlorate or nitrate, ...) were from Merck or Fluka.

The high temperature treatments were performed in a Pyrox HM 40 furnace using alumina boats up to 1100–1320°C under inert atmosphere in order to avoid the oxidization of tetravalent uranium into uranyl with a heating rate equal to 2–5°C min^{-1}.

The electron probe microanalyses (EPMA) were carried out using a Cameca SX 50 apparatus using an acceleration voltage of 15 kV and a current of 10 nA. The diameter of the analytical spot was equal to about 1 μm. The following calibration standards were used: ThO_2 (M_α ray of thorium), UO_2 (M_β ray of uranium) and $Ca_{10}(PO_4)_6(OH)_2$ (K_α ray of phosphorus).

The X-ray powder diffraction diagrams were collected with a Philips PW 1050/70 diffractometer using the Cu K_α ray ($\lambda = 1.5418$ Å). The patterns were recorded from 10° to 60° (2θ) each 0.01° with an acquisition time equal to 0.3 s step^{-1}. The identification of the phases was performed by interrogating the JCPDS – International Center for Diffraction Database and the DIFFRACT-AT search program supplied by Siemens and constraining the search to the elements involved in the synthesis and in the leaching tests. For all the solids studied, the unit cell parameters were refined using the U-Fit program [15].

The UV–visible absorption spectra were recorded with a Varian DMS 300 spectrophotometer. Powdered samples deposited on an adhesive tape which does not present any absorption bands between 300 and 900 nm. The infrared spectra were collected with a Hitachi I-2001 spectrophotometer (400–4000 cm^{-1}). The samples were ground in KBr (2–3 wt%) then pressed at 300 MPa.

The grain size distribution was determined with a Coulter LS 230 granulometer and the specific surface area was measured using the BET method (nitrogen adsorption) with a Coulter SA 3100 apparatus. Before making these experiments, the samples were dried for 10 h at 100°C.

Polytetrafluoroethylene (PTFE) containers were chosen for the leaching experiments at 90°C while for room temperature experiments, they were in high density polyethylene (HDPE). We verified that, in these conditions, less than 1% of the total dissolved element is adsorbed onto the surface of the containers.

The uranium and thorium concentrations were determined in the leachate by α-liquid scintillation with rejection of β/γ emitters using the Photon Electron Alpha Rejecting Liquid Scintillation (PERALS) spectrometer supplied by Ordela (Oak Ridge, TN, USA).

The phosphorus concentration was measured using capillary electrophoresis. It was a modular system consisting of a Spectraphoresis 100 injector (hydrodynamic mode) coupled with a high voltage (0–30 kV) power supply (Prime Vision VIII from Europhor) and a scanning UV–visible detector (Prime Vision IV from Europhor). In the present study, a voltage of 25 000 V resulting in an electric field of 333 V cm^{-1} was applied

and the wavelength was fixed to 214 nm. During the experiments, the temperature was maintained to 25°C. The acquisition and the treatment of the data were performed using the chromatography software BORWIN (developed by JMBS). Silica capillary (Supelco) was used. Prior to making the measurements, they were washed successively with 0.1M NaOH, deionized water then with the buffer solution. In order to confirm the results obtained, the phosphorus concentration were also determined using ICP-AES (Ultima apparatus from Jobin–Yvon). The results presented correspond to the average value of at least three determinations.

The TEM–STEM investigations were performed using either a Philips TEM 400 (High resolution stage) or a Philips CM 12 electron microscope (STEM). All the TEM modes at 120 keV were used: bright field (BF), dark field (DF), selected area diffraction (SAD), nanodiffraction (ND) and lattice fringes (LF). The dark field mode was used following the principle of azimutal and radial exploration of the reciprocal space, as more extensively described by Oberlin [16]. Taking into account the width (1.9 nm^{-1} in the reciprocal space) and the location of the objective aperture (2.5 nm^{-1}), the DF position admitted beams scattered in the $1.15 - 3.05$ nm^{-1} range. In the normal space, DF potentially revealed planes between 0.87 and 0.328 nm, respectively. The radial exploration showed the presence (or absence) of isotropy and the degree of crystallinity of the phases observed from well crystallized to amorphous. For amorphous compounds, the material always appeared softly illuminated for different radial positions $(0°, 45°, 90°)$ while crystals (under Bragg conditions) appeared white for one position and dark for the others. For amorphous materials, the size bright dots led at zero while it led up to crystallite size for crystalline materials [17]. STEM was performed to reveal the qualitative composition of the different phases. The aquisition parameters were a 20° tilt with a 15 nm spot size and a constant time equal to 1 ms for a matrix image of 512×400 points. X-energy dispersive spectroscopy (X-EDS) spectrum was previously monitored for semi-quantitative information. The X-EDS detector (CM12) was an EDAX super Ultra Thin Window (UTW) of 300 nm thickness. This detector with a 40 nm aluminum film, a metal layer of 27 nm and a silicon dead layer of 85 nm thick was characterized by a 164.41 eV resolution in energy. During the acquisition, the dead time was monitored to about 20–30%. This set-up conditions allows an optimized acquisition. In the lack of standards, only semi-quantitative results were obtained.

2.2. Syntheses of TUPD solid solutions

The TUPD solid solutions ($Th_{4-x}U_x(PO_4)_4P_2O_7$) were prepared using wet and dry chemistry methods [8–11]:

- In the first series of syntheses, thorium and tetravalent uranium chloride solutions were first mixed with concentrated phosphoric acid considering the initial mole ratios $U/Th = x/(4-x)$ and $(U+Th)/PO_4 = 2/3$. The samples were slowly evaporated between 100°C and 200°C, then ground and heated at 1250°C in argon atmosphere. For $x \leqslant 2$, ethanol was added to the mixture in order to increase the kinetic of precipitation of the solid then to avoid the oxidization of tetravalent uranium into uranyl during the evaporation step. The reaction can be given by the following global process

$$(4-x)\ ThCl_4 + xUCl_4 + 6\ H_3PO_4 \rightarrow Th_{4-x}U_x(PO_4)_4P_2O_7 + 16\ HCl\uparrow + H_2O\uparrow . \quad (1)$$

- In the second series of experiments, powdered samples of uranium (IV) diphosphate (α-UP_2O_7) and thorium phosphate–diphosphate (TPD) were first synthesized separately at high temperature ($\theta \leqslant 1200$°C), mixed, ground in a mortar, then heated at 1250°C several times in order to get the reaction [11].

$$(8-2x)\ Th_4(PO_4)_4P_2O_7 + 8x\ \alpha\text{-}UP_2O_7 \rightarrow 8\ Th_{4-x}U_x(PO_4)_4P_2O_7 + xP_4O_{10}\uparrow . \quad (2)$$

2.3. Characterization of the TUPD solid solutions

The TPD crystallizes in an orthorhombic system (space group *P*cam) with the following unit cell parameters: $a = 12.8646(9)$ Å, $b = 10.4374(8)$ Å, $c = 7.0676(5)$ Å [5]. For TUPD solid solutions, we observed the linear decrease of the unit cell parameters when increasing the substitution rate (JCPDS files no. 86–669 and 50–1862 to 50–1865) [10]. It confirmed the replacement of thorium by tetravalent uranium which is smaller ($^{[8]}r_{Th}^{4+} = 1.05$ Å and $^{[8]}r_{U}^{4+} = 1.00$ Å) in the TPD structure. The variations of the unit cell parameters and cell volume of $Th_{4-x}U_x(PO_4)_4P_2O_7$ were already described as a function of x in our published works [6,10,11]. From this study, it appeared that the TPD structure allows the replacement of thorium by large amounts of tetravalent uranium (up to $x = 3$). The maximum weight loading reaches 47.6 wt% (i.e. 75 mol%). In these conditions, solid solutions were synthesized up to $ThU_3(PO_4)_4P_2O_7$. For higher x values, polyphase systems were obtained. They were composed of $U_2O(PO_4)_2$ or $U_{2-x}Th_xO(PO_4)_2$, α-UP_2O_7 or α-U_{1-y}-$Th_yP_2O_7$ and $Th_{4-x}U_x(PO_4)_4P_2O_7$ after heating between 1150°C and 1350°C under inert atmosphere.

The unleached TUPD solid solutions used for the dissolution experiments were also characterized by EPMA. The elementary wt% and mole ratios of the

Table 1
Electron probe microanalysis results of the unleached TUPD ($x = 3.0$)

Element	Calc.[a]	Exp.
U (wt%)	47.6	47.8 ± 0.5
Th (wt%)	15.5	15.2 ± 0.5
P (wt%)	12.4	12.4 ± 0.2
O (wt%)	24.5	24.6 ± 0.2
Mole ratio		
Th/U	0.33	0.33 ± 0.01
$(U + Th)/PO_4$	0.67	0.66 ± 0.03

[a] Calculated considering the formula: $ThU_3(PO_4)_4P_2O_7$.

unleached $ThU_3(PO_4)_4P_2O_7$ are gathered in Table 1. They are in very good agreement with the values expected from the general formula.

Powdered samples of $ThU_3(PO_4)_4P_2O_7$ and $Th_3U(PO_4)_4P_2O_7$ were used for dissolution experiments. After grinding then heating at 1150°C for 10 h, the average grain size was equal to about 10 μm while the specific surface area reached 0.8 $m^2\ g^{-1}$. The specific surface area decreased to 0.2–0.3 $m^2\ g^{-1}$ when heating at 1250°C [13].

2.4. Leaching tests procedure and analysis of the leachate

Since the TPD (and TUPD) dissolution is very slow, several leaching tests were achieved in very corrosive media at constant temperature for several months in order to increase the dissolution rate and to reveal the formation of neoformed phases. For each dissolution experiment, samples of 100–700 mg of powdered or sintered TUPD were put into 5 ml of acidic solution (10^{-1} M–10^{-4} M HNO_3, 10^{-1} M $HClO_4$) then shaken for several days to few months. The ionic strength was kept constant ($I = 0.1$ M) by addition of sodium nitrate (or sodium perchlorate). At regular intervals, both phases were separated by centrifugation at 2000 rpm then at 13 000 rpm. A small part of the leachate (usually 100–200 μl) was removed then analyzed. The pH of the leachate was determined. The uranium activity was measured in solution by α-liquid scintillation (PERALS spectrometry) using a liquid–liquid extraction step by the tri-ni-octylphosphine oxide in 0.5 M H_2SO_4 (URAEX cocktail) [18]. In these conditions, the recovery of uranium reached 97–100% for a volume ratio between organic and aqueous phases equal to 0.25 [18]. The total phosphate concentration was also determined after the complete dissolution of the TUPD solids using capillary electrophoresis and ICP-AES.

A slightly higher release was initially observed because of the surface heterogeneity of unwashed minerals (minor phases, non-stoichiometry at the surface, particle size inferior to 1 μm, ...). This problem was avoided by the washing step. This step was performed at 25°C for several days in 10^{-1}–10^{-4} M $HClO_4$. Moreover, considering the corrosive medium we used, the surface irregularities were rapidly eliminated and, by this way, no significant increase was noted at the beginning of the dissolution curves.

Since only 1–2% of the leachate was renewed, which corresponds to a leaching flow equal to 6.0×10^{-2} ml $m^{-2}\ d^{-1}$, we supposed that the system solution–solid was not perturbed by the removing.

3. Theoretical section

3.1. Definition and expression of the normalized leaching and the normalized leaching (or dissolution) rate

3.1.1. Expression of the normalized leaching

The leachability of the element i from a mineral (in our case, i is one of the elements contained in the TUPD, i.e., usually thorium, uranium or phosphorus) can be described by its normalized leaching, $N_L(i)$(g m^{-2}), which is defined by the relation [7]

$$N_L(i) = \frac{\Delta m_{i\,sol.}}{f_i S} = \frac{m_i}{f_i S}, \tag{3}$$

where m_i is the total amount of i measured in solution (g), S the corresponding solid area (m^2), $\Delta m_{i\,sol.}$ corresponds to the mass loss of i in the solid and f_i is the mass ratio of the element i in the solid.

For a congruent dissolution (all the elements are dissolved with the same normalized dissolution rate and do not form neoformed phases in the back-end of the initial dissolution process), the mass of matrix dissolved can be calculated directly from the concentration of each element i measured in the leachate (in our case, uranium concentration). In the following sections, we assumed that the normalized dissolution rates of TUPD were determined during a congruent dissolution step which was proved for TPD in the first part of the dissolution curves [7].

3.1.2. Dependence of the normalized leaching on the leaching time – definition of the normalized leaching (or dissolution) rate

The expression of the normalized dissolution rate can be deduced from the evolution of the normalized leaching. Using the approach described by Lasaga [19], the normalized dissolution rate of the solid, R_L (g $m^{-2}\ d^{-1}$) can be written

$$R_L = \frac{1}{S}\frac{dm}{dt}, \tag{4}$$

which becomes

$$R_L = \frac{1}{f_i S}\frac{dm_i}{dt} = \frac{dN_L(i)}{dt} \tag{5}$$

Table 2
n values reported for several minerals

Mineral	*n*	pH range	Reference
Olivine	0.56	$2 \leqslant pH \leqslant 6$	[29]
Albite	0.49	$2 \leqslant pH \leqslant 6$	[20]
Diopsite	0.70	$2 < pH < 6$	[31]
Enstatite	0.80	$2 < pH < 6$	[21]
Anorthite	0.54	$2 \leqslant pH \leqslant 5.6$	[21]
TUPD	0.40 ± 0.02	$2 \leqslant pH \leqslant 4$	This work
TPD: Cm^{3+}	0.31 ± 0.01	$1 \leqslant pH \leqslant 3$	[39–41]
TPD : Am^{3+}	0.35 ± 0.04		
TPPD	N.S.[a]	$1 \leqslant pH \leqslant 4$	[39–41]

[a] Not significant due to the precipitation of a tetravalent plutonium phosphate [7].

when the dissolution is congruent. From the literature, it appears that the normalized dissolution rate (i.e. the slope obtained when plotting the normalized leaching versus time) is constant for several minerals [20–24]. In the case of unwashed minerals, parabolic rate laws were observed because of the heterogeneity in the surface properties (different phases, different particle sizes). As already discussed, we avoided this phenomenon by washing the solid prior to perform the leaching tests.

In acidic medium the normalized dissolution rate R_L is usually noted R_H, while in basic medium it is often noted R_{OH}. Since all the leaching experiments were performed in acidic media for this study, we will use the R_H notation in the following sections.

3.1.3. Influence of the temperature on the normalized dissolution rate

In our previous works concerning the leaching tests performed on the pure TPD [7], we already found that the normalized dissolution rate depends on temperature according to the Arrhenius law, i.e.,

$$R_H = k\ e^{\left(-\frac{E_{app}}{RT}\right)}, \tag{6}$$

where k is the normalized dissolution rate constant independent of the temperature (g m^{-2} d^{-1}) and E_{app} is the apparent activation energy of the dissolution of the mineral (kJ mol^{-1}). Since the temperature dependence of the rate law for the overall dissolution may be more complex than the temperature dependence of an elementary reaction, this appellation was chosen to make the difference with the classical activation energy as already discussed by Lasaga [25].

3.1.4. Influence of the proton concentration on the normalized dissolution rate

Several authors investigated the dissolution reactions between minerals and aqueous solutions from a kinetic point of view [26–29]. These authors studied the dependence of the normalized dissolution rate on the pH and showed experimentally that R_H can be written

$$R_H = k'_T(a_{H_3O^+})^n, \tag{7}$$

where k'_T corresponds to the apparent normalized dissolution rate constant dependent on temperature (g m^{-2} d^{-1}); $a_{H_3O^+}$ refers to the protons activity and n is the partial order related to H_3O^+ ions.

The experimental n values obtained for most of the minerals are usually in the range $0 < n < 1$ as reported in Table 2 [7,29–32]. Several explanations based on the transition state theory [19,28] or on the coordination chemistry involving surface proton concentration [26,27,29] were given. Furthermore, we can note that the n value depends on the kinetic mechanism but does not correspond to the number of protons involved in the global reaction of dissolution. Moreover, Eq. (7) implies the proton activity. Nevertheless, in most of the cases, it is easier to use the proton concentration. Introducing the proton activity coefficient, Eq. (7) becomes

$$R_H = k'_T(\gamma_{H_3O^+}[H_3O^+])^n = k'_{T,I}[H_3O^+]^n. \tag{8}$$

In this expression, $k'_{T,I}$ represents the apparent normalized dissolution rate constant for proton-promoted dissolution defined for $pH < 7$ and $\gamma_{H_3O^+}$ corresponds to the proton activity coefficient. $k'_{T,I}$ is independent of the pH (its value corresponds to $pH = 0$), but it is dependent on the temperature, the medium and the ionic strength (I).

4. Results and discussion

4.1. Kinetic study of the TUPD dissolution

4.1.1. Influence of the temperature on the normalized dissolution rate

Leaching tests were performed at 25°C and at 90°C in order to determine the apparent activation energy of the TUPD dissolution. The preliminary results led to an activation energy equal to about 40 kJ mol^{-1}. This result

needs to be confirmed since the normalized dissolution rates obtained at room temperature are very low and the corresponding uncertainties are rather high even after 3 years of leaching. Nevertheless, it is in good agreement with the value obtained when leaching pure TPD in 5 M HNO_3 (42 ± 3 kJ mol^{-1}) or thorium–plutonium (IV) phosphate–diphosphate solid solutions (TPPD) in distilled water (41 ± 1 kJ mol^{-1}) [7,33]. Moreover, this value is very close to that reported for several minerals [34–38]. It could indicate the existence of an activated complex which adsorption energy on the surface of the sample could reduce the apparent activation energy measured considering Eq. (6).

4.1.2. Influence of the proton concentration on the normalized dissolution rate

Leaching tests were performed at 90°C in several acidic solutions. The evolution of the normalized leaching $N_L(U)$ in 10^{-2}, 10^{-3} and 10^{-4} M HNO_3 are reported in Fig. 1. For all the samples, three dissolution steps were observed on the dissolution curves:

- Linear increase of $N_L(U)$ as well as of the total amount of dissolved matrix;
- Strong increase of $N_L(U)$ simultaneously with the pH decrease (pH = 1.6 at equilibrium);
- Decrease of the uranium concentration measured in the solution which reaches a plateau.

We must note that the normalized leaching $N_L(U)$ is only representative of the TUPD dissolution during the two first steps. Indeed, even though these two steps correspond to a kinetic process, the third one is thermodynamically controlled since it is due to the formation of secondary phases as discussed in the following section.

In these conditions, the normalized dissolution rates were calculated from the first part of the dissolution curves in order to determine the partial order related to the proton concentration and the apparent normalized dissolution rate constant considering Eq. (7).

Table 3
R_H, $k'_{T,I}$ and n values obtained for $ThU_3(PO_4)_4P_2O_7$ at 90°C

Leachate	R_H (g m^{-2}d^{-1})
10^{-1} M HNO_3	N.S.[a]
10^{-2} M HNO_3	$(5.0 \pm 0.9) \times 10^{-5}$
10^{-3} M HNO_3	$(1.7 \pm 0.2) \times 10^{-5}$
10^{-4} M HNO_3	$(6.9 \pm 0.7) \times 10^{-6}$
n	0.40 ± 0.02
$k'_{363K,0.1M}$ (g m^{-2} d^{-1})	$(2.8 \pm 0.7) \times 10^{-4}$

[a] Not significant because of the rapid oxidization of U^{4+} into uranyl.

The n and $k'_{T,I}$ values, as well as the dissolution rates R_H determined in 10^{-2}, 10^{-3} and 10^{-4} M HNO_3 at 90°C, are summarized in Table 3 while the variation of log (R_H) versus log [H_3O^+] is plotted in Fig. 2. The n value obtained ($n = 0.40 \pm 0.02$) is rather consistent with those determined for TPD doped with trivalent actinides in nitric acid at room temperature (0.31–0.35) and for several other minerals as shown in Table 2 [7,33,39–41].

We also studied the influence of the background salt on the dissolution of TUPD solid solutions. In this aim, TUPD sample was leached in 10^{-1} M $HClO_4$ at 90°C. In this medium, the dissolution rate is smaller than that obtained in 10^{-1} M $HClO_4$ as shown in Fig. 3. This difference can be due to the strong oxidization rate of tetravalent uranium into uranyl in nitric medium.

4.2. Thermodynamic study of the TUPD dissolution: observation and characterization of the neoformed phases

As already discussed, the second step observed during the leaching process is characterized by the increase of the normalized dissolution rate probably because of the pH decrease from the initial value down to the pH

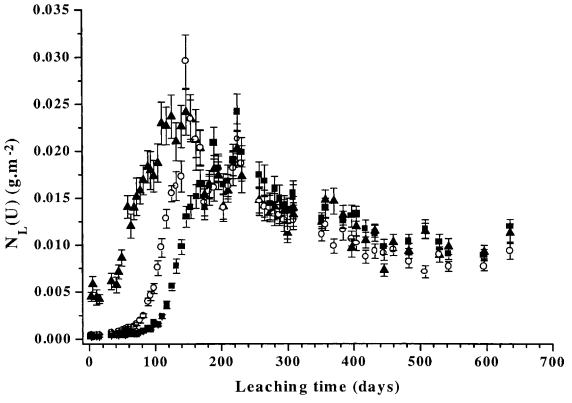

Fig. 1. Evolution of $N_L(U)$ for leaching tests of TUPD in HNO_3 at 90°C (▲) 10^{-2} M; (○) 10^{-3} M; (■) 10^{-4} M.

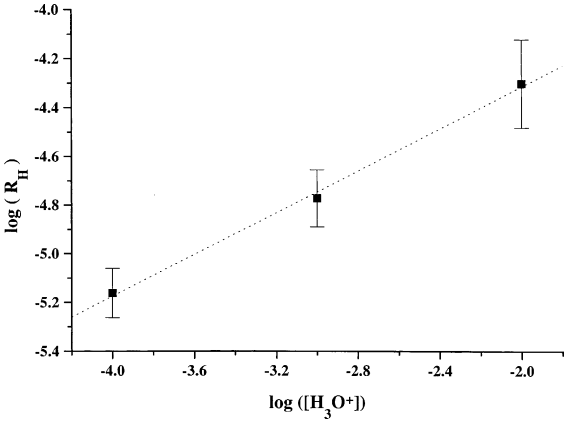

Fig. 2. Variation of log(R_H) versus log[H_3O^+] at 90°C.

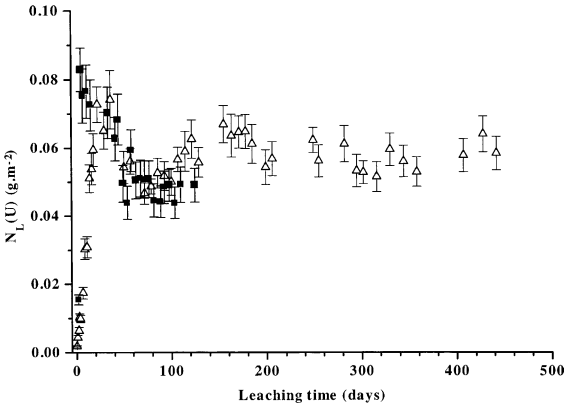

Fig. 3. Evolution of $N_L(U)$ for TUPD in 10^{-1} M HNO_3 (■) and 10^{-1} M $HClO_4$ (△) at 90°C.

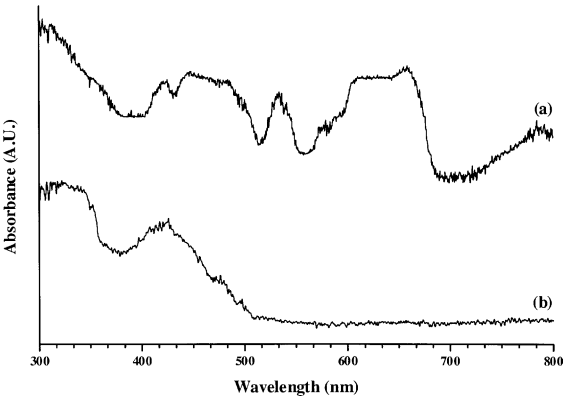

Fig. 4. UV–visible spectra of the unleached (a) and leached TUPD (b) (10^{-1} M HNO_3, $\theta = 90$°C).

value obtained at equilibrium (pH = 1.6). When increasing the leaching time, the initial green colored solid solution slowly turned into yellow colored powder (which is characteristic of uranyl ions). Correlatively, the uranium concentration reached a plateau. This phenomenon was assigned to the precipitation of neoformed phase in undersaturation conditions. It is also probably responsible of the pH variations observed. After these two first dissolution steps controlled by the kinetics, the third one (which corresponds to the stabilization of the uranium concentration in the leachate) seems to be controlled by thermodynamics leading to the precipitation of a neoformed phase containing uranyl and phosphate ions. The residues obtained after the complete dissolution of the solids were separated from the leachate by centrifugation, washed with deionized water, filtered, dried then characterized using the techniques previously mentioned. As a comparison, three other uranium phosphates: $U_2O(PO_4)_2$, $U(UO_2)(PO_4)_2$ and α-UP_2O_7 were leached in the same conditions (10^{-1} M $HNO_3, \theta = 90$°C) in order to get a better understanding of the results obtained for TUPD solid solutions.

4.2.1. Characterization of the phases neoformed at the saturation of the solution using UV–visible and infrared spectroscopies, XRD and EPMA

The residue obtained after the complete dissolution of TUPD solid solutions was first characterized by UV–visible spectroscopy in order to reveal the presence of uranyl groups and to confirm whether all the initial tetravalent uranium was oxidized during the leaching process. The UV–visible spectrum of the unleached and leached TUPD are reported in Figs. 4(a) and (b), respectively. The comparison of both spectra clearly revealed the presence of the absorption bands of U^{4+} for the unleached TUPD ($^3P_2$: 420 nm; $^1I_6$: 435–490 nm; ^3P_I : 500–600 nm; $^1G_4$,$^1D_2$ and $^3P_0$: 560–690 nm and $^3H_6$: 800 nm) as already reported in our previous papers [11,42–44]. Correlatively, all these bands disappear on the UV–visible spectrum of the leached TUPD. Simultaneously, a broad band characteristic of UO_2^{2+} groups observed between 380 and 500 nm confirms that the tetravalent uranium is oxidized during the leaching tests.

The leached TUPD (10^{-1} M $HNO_3, \theta = 90$°C, $t = 500$ days) was also characterized using XRD. The diffraction patterns of the residue obtained after the complete dissolution of other tetravalent uranium phosphates like $U_2O(PO_4)_2$ and $U(UO_2)(PO_4)_2$ in 10^{-1} M HNO_3 confirmed the neoformation of the uranyl phosphate tetrahydrate $(UO_2)_3(PO_4)_2 \cdot 4H_2O$ reported in the literature (JCPDS files no. 13–39 and 37–369). Its XRD diagram is presented in Fig. 5(c). Nevertheless, a recent study concerning the uranyl vanadate pentahydrate $(UO_2)_3(VO_4)_2 \cdot 5H_2O$ revealed that this compound crystallizes with five water molecules [45]. The XRD diagram obtained after the complete dissolution of $U_2O(PO_4)_2$ and $U(UO_2)(PO_4)_2$ showed that the solid neoformed is isostructural with $(UO_2)_3(VO_4)_2 \cdot 5H_2O$. All diffraction lines were indexed by analogy with the results reported by Saadi et al. [45] for $(UO_2)_3(VO_4)_2 \cdot 5H_2O$ as shown in Table 4. For this reason, we prefer the formulation $(UO_2)_3(PO_4)_2 \cdot 5H_2O$ instead of $(UO_2)_3(PO_4)_2 \cdot 4H_2O$ since the electron probe microanalysis (Table 5) did not allow one to determine the number of water molecules with a good accuracy (it was found between 4 and 5) due to the presence of uranium or/and thorium of high Z values in the solid analyzed. However, the structure of the uranyl vanadate hydrate clearly shows the presence of five water molecules in the polyhedron of one of the two types of the uranyl environment.

The leaching experiments of the two uranium phosphates led to a yellow colored precipitate after the complete dissolution of the initial solids. The EPMA

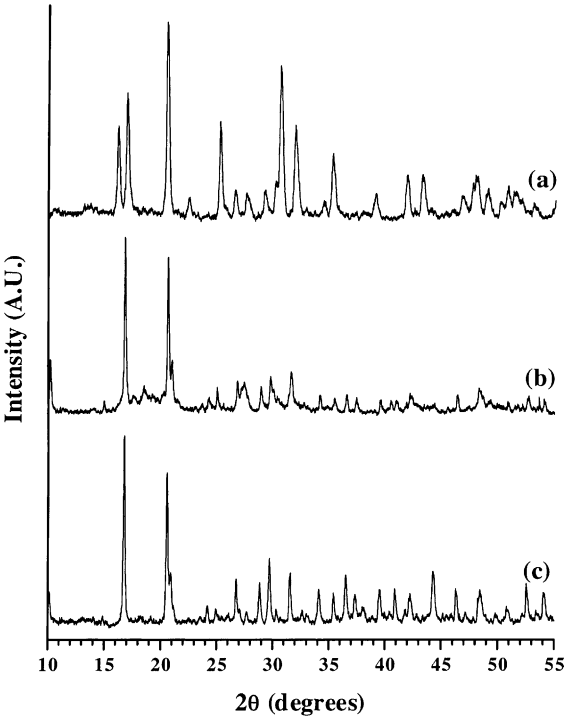

Fig. 5. XRD diagram of unleached TUPD (a), leached TUPD (b) and leached $U(UO_2)(PO_4)_2$ (c) (10^{-1} M HNO_3, $\theta = 90°C$).

results of the secondary phase are summarized in Table 5. They are consistent with the phase previously described. The elementary wt% as well as the mole ratios determined correspond to those calculated from $(UO_2)_3(PO_4)_2 \cdot 5H_2O$. The uranium diphosphate α-UP_2O_7 was also leached in 10^{-1} M HNO_3 at 90°C in order to verify whether the nature of phosphate has an influence on the precipitation of $(UO_2)_3(PO_4)_2 \cdot 5H_2O$. No difference was observed. Thus, this study underlined the chemical instability of the $P_2O_7^{4-}$ group in these conditions.

The XRD diagram of the solid obtained after dissolution of TUPD (Fig. 5(b)) is completely different to that of the unleached TUPD (Fig. 5(a)). Moreover, the comparison of this diagram with that of $(UO_2)_3(PO_4)_2 \cdot 5H_2O$ revealed some great similarities. Additional diffraction lines were observed on the diagram obtained after dissolving the TUPD solid solutions. They can be assigned to the thorium phosphate–hydrogenphosphate monohydrate by comparison to the results obtained starting from thorium and phosphate ions in the mole ratio $r = Th/PO_4 = 2/3$ and using hydrothermal conditions as already discussed in our published works [7,46]. The system was thus composed by $(UO_2)_3(PO_4)_2 \cdot 5H_2O$ and $Th_2(PO_4)_2HPO_4 \cdot H_2O$ which was also confirmed by the electron probe microanalysis on the TUPD sample leached in 10^{-1} M HNO_3 at 90°C (Table 6).

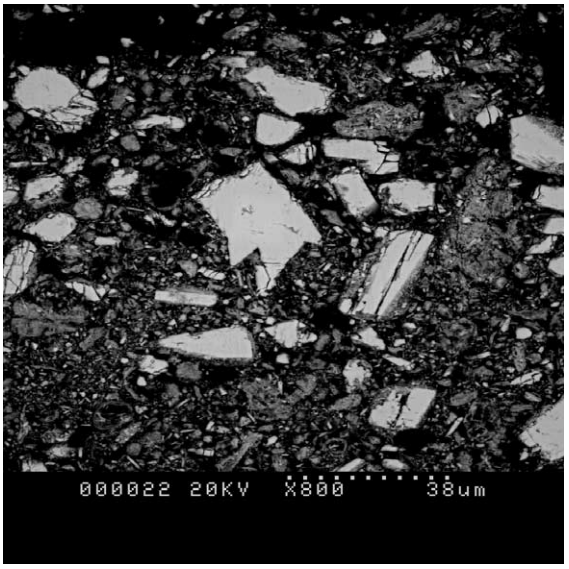

Fig. 6. SEM backscattered micrograph obtained after the complete dissolution of TUPD (10^{-1} M HNO_3, $\theta = 90°C$).

This analysis confirmed that the initial TUPD was completely dissolved during the leaching experiments. The final solid obtained corresponds to a two-phase system. The first phase (light phase in the SEM backscattered micrograph, Fig. 6) was identified as the uranyl phosphate pentahydrate $(UO_2)_3(PO_4)_2 \cdot 5H_2O$. The experimental elementary wt% obtained for each element and the corresponding mole ratios in this phase are in good accordance with those calculated from the global formula proposed.

The second phase (dark phase in the SEM micrograph, Fig. 6) seems to correspond to a two-phase system containing small amounts of crystallized $(UO_2)_3(PO_4)_2 \cdot 5H_2O$, on one hand, and thorium phosphate–hydrogenphosphate hydrate, on the other hand. Considering that all uranium content in the dark phase is present as $(UO_2)_3(PO_4)_2 \cdot 5H_2O$, it was possible to determine the elementary wt% and the corresponding mole ratios in the second phase. They are equal to 21.8 ± 0.8 and to 4.5 ± 0.2 for Th and P, respectively. This result leads to a mole ratio Th/P close to 0.65. This mole ratio is in good agreement with that found during the leaching tests of pure TPD in 5M HNO_3 as described previously [7]. In these conditions, the presence of thorium phosphate–hydrogenphosphate, $Th_2(PO_4)_2HPO_4 \cdot H_2O$, was proved. As reported in the following section, the TEM analysis performed on this polyphase system also confirmed the results obtained from XRD and EPMA.

On the SEM micrographs reported in Fig. 7, two kinds of particles are observed. These particles differ from their size, shape and appearance. Elongated

Table 4
Indexing of the diffraction lines of $(UO_2)_3(PO_4)_2 \cdot 5H_2O$ obtained on the XRD diagram

h	k	l	$2\theta_{obs.}$(deg)	$2\theta_{calc.}$(deg)	$d_{obs.}$(Å)	I/I_0
1	1	0	8.46	8.485	10.44	30
2	0	0	10.35	10.375	8.54	80
1	1	1	15.12	15.128	5.85	5
2	2	0	17.00	17.016	5.22	100
0	2	1	18.40	18.403	4.82	5
4	0	0	20.82	20.836	4.26	70
2	2	1	21.16	21.170	4.19	25
1	3	1	24.42	24.427	3.642	10
0	0	2	25.18	25.155	3.530	10
5	1	0	26.98	27.006	3.302	40
4	2	1	27.90	27.937	3.195	10
2	4	0	29.06	29.081	3.068	35
0	4	1	29.92	29.937	2.984	35
3	1	2	30.52	30.512	2.927	5
2	4	1	31.80	31.764	2.812	20
4	0	2	32.87	32.885	2.722	5
6	2	0	34.35	34.369	2.609	30
4	2	2	35.65	35.675	2.516	15
4	4	1	36.77	36.758	2.442	25
7	1	0	37.64	37.547	2.388	30
3	5	1	39.85	39.819	2.260	15
0	6	0	41.15	41.137	2.192	30
6	4	0	41.99	42.001	2.150	10
8	0	0	42.39	42.404	2.131	20
6	4	1	44.01	43.993	2.056	5
2	6	1	44.53	44.514	2.033	10
4	6	0	46.55	46.549	1.949	30
9	1	0	48.55	48.543	1.874	20
7	5	1	52.80	52.802	1.732	20
9	3	1	54.29	54.304	1.688	15
0	8	0	55.82	55.866	1.646	15
2	8	0	57.00	56.990	1.614	10
2	8	1	58.61	58.596	1.574	10

Table 5
Electron probe microanalysis of the solid obtained after the complete dissolution of $U(UO_2)(PO_4)_2$ or $U_2O(PO_4)_2$ (10^{-1} M HNO_3, $\theta = 90°C$)

Element	Calc.[a]	Exp.[b]	Exp.[c]	Average value
Th (wt%)	–	–	–	–
U (wt%)	65.5	65.4 ± 1.2	67.0 ± 1.1	66.2 ± 1.2
P (wt%)	5.7	5.5 ± 0.1	5.5 ± 0.2	5.5 ± 0.2
O (wt%)	27.9	28.4 ± 1.2	26.8 ± 1.5	27.6 ± 1.4
In which O from water (wt%)	8.2	8.7 ± 0.7	6.8 ± 0.9	7.8 ± 0.8
PO_4/U	0.67	0.65 ± 0.02	0.63 ± 0.02	0.64 ± 0.02
P_2O/U	1.67	1.70 ± 0.20	1.35 ± 0.15	1.55 ± 0.20
Proposed formula			$(UO_2)_3(PO_4)_2 \cdot 5H_2O$	

[a] Calculated considering the formula $(UO_2)_3(PO_4)_2 \cdot 5H_2O$.
[b] Leaching of $U(UO_2)(PO_4)_2$.
[c] Leaching of $U_2O(PO_4)_2$.

orthorombic crystals of several micrometers long are uranium enriched and correspond to the uranyl phosphate pentahydrate $(UO_2)_3(PO_4)_2 \cdot 5H_2O$. The grain size of the second particle population is smaller (average particle size inferior at 2 μm) without specific shape. They appears as aggregates which seem to be deposited

Table 6
Electron probe microanalysis of the solid obtained after the complete dissolution of $ThU_3(PO_4)_4P_2O_7$ (10^{-1} M HNO_3, $\theta = 90°C$)

Element	Calc.[a]	Calc.[b]	Leached TUPD (first phase)	Leached TUPD (second phase)
Th (wt%)	–	60.4	0.5 ± 0.4	19.9 ± 1.8
U (wt%)	65.5	–	66.2 ± 0.5	36.3 ± 3.0
P (wt%)	5.7	12.1	5.7 ± 0.1	7.2 ± 0.2
O (wt%)	27.9	27.0	20.8 ± 0.3[c]	19.3 ± 0.5[c]
In which O from water (wt%)	8.2	2.3	7.3 ± 0.8	N.D.[d]
Th/U	–	–	<0.01	0.56 ± 0.09
$(Th + U)/PO_4$	1.50	0.67	1.52 ± 0.04	1.0 ± 0.2
Proposed formula			$(UO_2)_3(PO_4)_2 \cdot 5H_2O$	$(UO_2)_3(PO_4)_2 \cdot 5H_2O +$ $Th_2(PO_4)_2(HPO_4) \cdot H_2O$

[a] Calculated considering the formula $(UO_2)_3(PO_4)_2 \cdot 5H_2O$.
[b] Calculated considering the formula $Th_2(PO_4)_2(HPO_4) \cdot H_2O$.
[c] Excluding oxygen from water molecules.
[d] Not determined because of the high porosity observed due to the particle size (<1 μm).

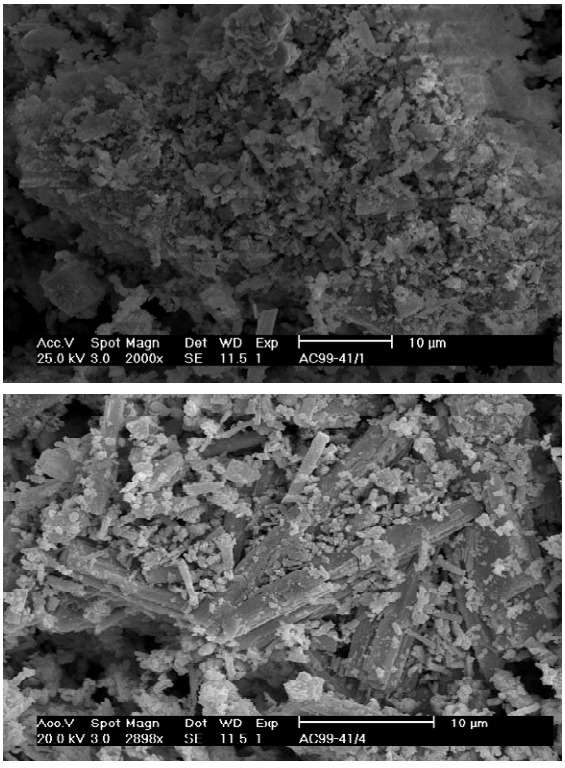

Fig. 7. SEM micrographs obtained after the complete dissolution of TUPD (10^{-1} M HNO_3, $\theta = 90°C$).

onto the orthorhombic crystals. They look like the particles observed when leaching pure TPD in the same conditions. These small particles are thorium enriched and can be identified to the thorium phosphate–hydrogenphosphate $Th_2(PO_4)_2HPO_4 \cdot H_2O$. That is in good agreement with the results obtained from the SEM backscattered micrograph (Fig. 6) and the EPMA.

The residues obtained after dissolution of the initial solids were also characterized by infrared spectroscopy in order to verify the absence of the P–O–P bond characteristic of the diphosphate group clearly seen in the spectrum of the unleached $Th_3U(PO_4)_4P_2O_7$ [5]. The spectra obtained for the leached $U_2O(PO_4)_2$ or $U(UO_2)(PO_4)_2$ and TUPD are reported in Figs. 8(a)

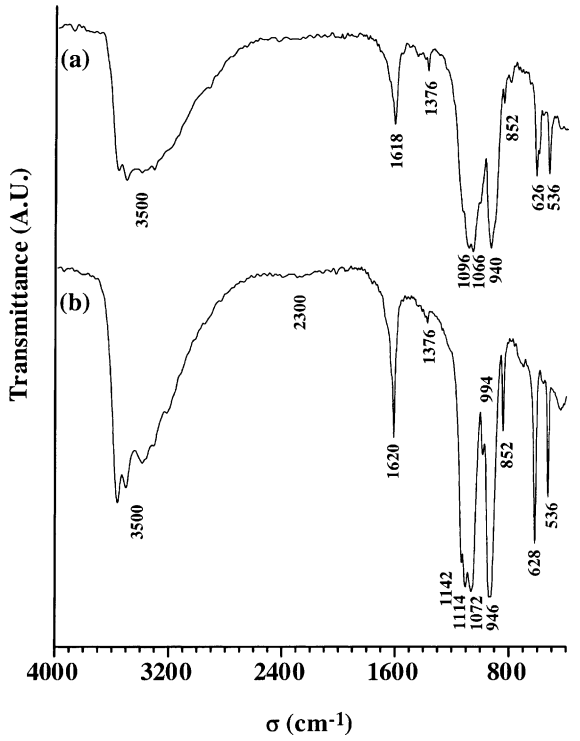

Fig. 8. IR spectra of leached $U(UO_2)(PO_4)_2$ (a) and leached TUPD (b) (10^{-1} M HNO_3, $\theta = 90°C$).

and (b), respectively. The diphosphate group can be decomposed in two pyramids and a central bridge P–O–P. The two stretching modes are generally IR active when the P–O–P bond is not linear. A study of the spectrum of the uranium (IV) diphosphate α-UP_2O_7 allowed to assign the band at 737 cm^{-1} to the v_s (P–O–P) stretching mode, while v_{as} (P–O–P) was found at about 950 cm^{-1} [42]. The assignment of the bands observed in the infrared spectra of the leached TUPD confirmed the absence of diphosphate groups in the polyphase system finally obtained as shown from Table 7. The presence of a weak shoulder at about 2300 cm^{-1} was assigned to the (P)–O–H antisymmetric stretching mode due to the presence of the thorium phosphate–hydrogenphosphate $Th_2(PO_4)_2HPO_4 \cdot H_2O$. In both spectra, we assigned the band observed at 1376 cm^{-1} to the remaining adsorbed nitrate ions on the surface of the solids formed during the leaching tests in nitric acid.

The stretching mode of the uranyl group (UO_2^{2+}) are usually IR active [47–49]. For $(UO_2)_3(PO_4)_2 \cdot 5H_2O$, Pekarek and Vesely [49] assigned the frequencies observed at 845 and 930 cm^{-1} to the stretching modes v_1 and v_3. On the infrared spectrum presented in Fig. 8, we observed these stretching modes at 852 and 940 cm^{-1}, respectively. Moreover, the study of 31 uranyl compounds gave the linear relation between the v_1 and v_3 frequencies [50–52]. Another study conducted by Bartlett and Cooney [53] on IR and Raman spectra of 27 uranyl compounds gave the relations between v_3 (expressed in cm^{-1}) and the U=O length bond $R_{U=O}$ (expressed in pm), on one hand, and between v_1 and $R_{U=O}$, on the other hand, as follows:

$$R_{(U=O)} = 10650(v_1)^{-2/3} + 57.5, \tag{9}$$

$$R_{(U=O)} = 9141(v_3)^{-2/3} + 80.4. \tag{10}$$

Considering the v_1 and v_3 values obtained for $(UO_2)_3(PO_4)_2 \cdot 5H_2O$ (Fig. 8), the calculated $R_{U=O}$ was found to be equal to 176 and 175.3 pm from Eq. (9) and Eq. (10), respectively. That is in good agreement with the values usually reported for the UO_2^{2+} group [54] and with the value obtained for $(UO_2)_3(VO_4)_2 \cdot 5H_2O$ [45].

Table 7
Assignment of the bands observed in the infrared spectra of the leached and unleached TUPD and on the leached $U(UO_2)(PO_4)_2$

Frequency σ (cm^{-1})			Assignment
Unleached TUPD	Leached TUPD	Leached $U(UO_2)(PO_4)_2$	
436	448	450	δ_s(P–O) of PO_4^{3-} and HPO_4^{2-}
489, 527, 555, 638	536, 628	536, 626	δ_{as}(P–O) of PO_4^{3-} and HPO_4^{2-}
696, 752	N.O.[a]	N.O.[a]	v_s(P–O–P)
N.O.[a]	852	852	$v_1(UO_2^{2+})$
N.O.[a]	946	940	$v_3(UO_2^{2+})$
918	N.O.[a]	N.O.[a]	v_{as}(P–O–P)
970	994	940	v_s(P–O) of PO_4^{3-} and HPO_4^{2-}
1020–1200	1072,1114,1142	1066, 1096	v_{as}(P–O) of PO_4^{3-} and HPO_4^{2-}
N.O.[a]	1376	1376	v_{as}(N–O) of NO_3^- (adsorbed at the surface)
N.O.[a]	1620	1618	H_2O bending mode
N.O.[a]	2300	N.O.[a]	v_{as}((P)–O–H) of HPO_4^{2-}
N.O.[a]	3300–3600	3300–3600	H_2O stretching modes

[a] Not observed in the IR spectrum.

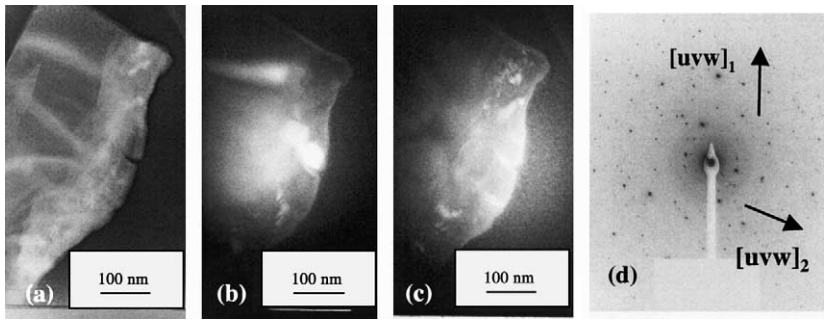

Fig. 9. Bright field (a), dark field 0° (b) and 90° (c) and selected area diffraction (d) of the raw TUPD.

4.3. Observation of the TUPD dissolution by TEM

4.3.1. Unleached TUPD

Bright field (Fig. 9(a): BF), dark field (Fig. 9(b)) and (c): DF and selective area diffraction (Fig. 9(d): SAD) were performed on the raw TUPD. The main characteristics of the TUPD were observed. A well crystallized materials with a SAD pattern typical of crystal is observed. The indexing gave the TUPD occurrence with a correlation coefficient between XRD and SAD data equal to 0.98. The DF revealed the presence of a very thin layer (2–5 nm) around the TUPD crystals which kept bright for two orthogonal radial positions of the objective aperture. In such case, this result implies that this layer is amorphous. It was probably generated during the manufacturing process and caused by a passive oxidization as observed in other ceramics [55]. On the contrary, the black arrows show very well crystallized materials which are alternatively bright and dark for two orthogonal positions of the objective aperture (in the radial study of the reciprocal space).

4.3.2. Leached TUPD

The leached TUPD exhibits a complex behavior. A mixture of several phases occurred rapidly. Three different phases were distinguished as illustrated in Fig. 10 from X-EDS mapping and SAD analyses. The first one is an uranium phase while the other ones are thorium phosphate phases. The well crystallized uranium phase with macrometric crystals gave an occurrence of $(UO_2)_3(PO_4)_2 \cdot 5H_2O$ which is in good agreement with the results already reported (Table 8). The thorium phases are more complex. Amorphous and crystallized phases were observed simultaneously by SAD. The SAD indexing of the crystallized phase gave an occurrence of thorium phosphate–hydrogenphosphate (TPHP) with grain size smaller than 1 μm. The X-EDS technique revealed that the amorphous phase is thorium enriched. It

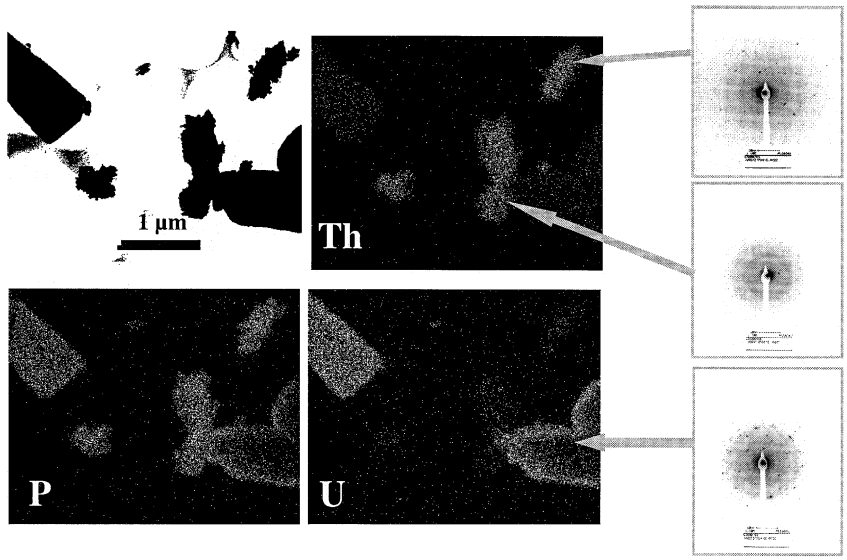

Fig. 10. STEM/X-EDS image and SAD of leached TUPD (10^{-1} M HNO_3, 90°C, 125 days).

Table 8
Nano-diffraction indexing for the neoformed $(UO_2)_3(PO_4)_2 \cdot 5H_2O$

$d_{mes.}$ (Å)	$d_{cals.}$ (Å)	h	k	l
5.23	5.211	2	2	0
4.05	4.195	2	2	1
3.30	3.302	5	1	0
3.06	3.068	2	4	0
2.96	2.984	0	4	1
2.86	2.812	2	4	1
2.41	2.388	7	1	0
	2.442	4	4	1

was identified as $Th_2(PO_4)_2HPO_4 \cdot xH_2O$. Small amounts of remaining uranyl phosphate pentahydrate was observed in this gelatinous phase (as already described in Table 6). Moreover, some thorium-uranyl were observed either by X-EDS and EPMA analysis. The EPMA analysis also revealed small amounts of an additional phase (<0.3 wt%) which was identified as a uranium-thorium hydrogenphosphate hydrate since the (U+Th)/PO_4 mole ratio was found to be equal to 1/2 while the mole ratio U/Th was not constant.

4.4. Determination of the solubility product of $(UO_2)_3(PO_4)_2 \cdot 5H_2O$

The characterization previously described showed that leaching tests of uranium phosphates compounds led to the uranyl phosphate pentahydrate. This solid seems to control the uranium concentration in the solution during the leaching tests of TUPD solid solutions (third part of the $N_L(U)$ evolution curves in Fig. 1). Since the reaction between $(UO_2)_3(PO_4)_2 \cdot 5H_2O$ and the solution is characterized by a real equilibrium, we were interested in the determination of the corresponding equilibrium constant (solubility product). The phosphorus ions concentrations measured after leaching the TUPD solid solutions in 10^{-2}, 10^{-3} and 10^{-4} M HNO_3 during 300 days of leaching time is given in Table 9. They were compared to those calculated from the uranium concentration measured in the leachate making the assumption that the dissolution of TUPD solid solution was stoichiometric and that the thorium ions mainly precipitate as a thorium phosphate–hydrogenphosphate (i.e. in the mole ratio Th/P = 2/3) which was already verified and discussed [7].

The reaction of formation of the uranyl phosphate pentahydrate $(UO_2)_3(PO_4)_2 \cdot 5H_2O$ can be written

$$(UO_2)_3(PO_4)_2 \cdot 5H_2O \leftrightarrow 3UO_2^{2+} + 2PO_4^{3-} + 5H_2O. \quad (11)$$

Three methods were used to determine the solubility product of $(UO_2)_3(PO_4)_2 \cdot 5H_2O$:

- The first way was based on the direct dissolution of $(UO_2)_3(PO_4)_2 \cdot 5H_2O$ in 10^{-1} M HNO_3. The uranium and phosphate concentrations were measured in the leachate when the thermodynamic equilibrium was reached.
- The second way consisted in evaluating this constant from the formation of the uranyl phosphate after the complete dissolution of three uranium phosphates studied: diuranium oxide phosphate $U_2O(PO_4)_2$, uranium-uranyl phosphate $U(UO_2)(PO_4)_2$ and uranium diphosphate α-UP_2O_7.

The phosphate content was calculated from the uranium concentration measured in the leachate when the equilibrium between the powdered $(UO_2)_3(PO_4)_2 \cdot 5H_2O$ and the solution was obtained and considering the U/PO_4 stoichiometry of the initial solid dissolved and that of the solid precipitated (Table 10).

- The third way of determination developed, concerned the leaching tests of TUPD in nitric acid solutions (Table 11).

The variation of the solubility product K_S° was extrapolated to a ionic strength equal to zero, $K_{S,0}^\circ$ using the specific-ion interaction theory and considering the data reported concerning the chemical thermodynamics of uranium by Ciavatta [56]. It can be expressed as a function of the molality m_X of the species X, the Debye–Hückel term D and the coefficients of interaction $\varepsilon(i,j)$ between the i and j species, as follows:

$$\log(K_S^\circ) = \log(K_{S,0}^\circ) - 3\log(\gamma_{UO_2^{2+}}) - 2\log(\gamma_{PO_4^{3-}}) - 5\log(a_{H_2O}). \quad (12)$$

In this expression

$$\log(\gamma_{UO_2^{2+}}) = -(z_{UO_2^{2+}})^2 D + \varepsilon_{(UO_2^{2+},X)} m_X, \quad (13)$$

Table 9
Phosphate concentration measured and calculated in the leachate

CPO_4	HNO_3 (10^{-2} M)	HNO_3 (10^{-3} M)	HNO_3 (10^{-4} M)
Calc.[a]	3×10^{-2} M	2.7×10^{-2} M	2.2×10^{-2} M
Exp.[b]	$(3.3 \pm 0.6) \times 10^{-2}$ M	$(3.3 \pm 0.6) \times 10^{-2}$ M	$(4.2 \pm 0.6) \times 10^{-2}$ M
Exp.[c]	$(3.0 \pm 0.4) \times 10^{-2}$ M	$(3.5 \pm 0.4) \times 10^{-2}$ M	$(3.8 \pm 0.4) \times 10^{-2}$ M

[a] Calculated considering the stoichiometry of the unleached TUPD and of $(UO_2)_3(PO_4)_2 \cdot 5H_2O$.
[b] Determined using capillary electrophoresis.
[c] Determined using ICP-AES.

Table 10
Determination of the solubility product, $K^{\circ}_{S,0}$, of $(UO_2)_3(PO_4)_2 \cdot 5H_2O$

Sample[a]	$C_{UO_2^{2+}}$ (M)	$C_{PO_4^{3-}}$ (M)	$[UO_2^{2+}]$ (M)	$[PO_4^{3-}]$ (M)	$\log([UO_2^{2+}]^3[PO_4^{3-}]^2)$ ($\theta = 90°C$, $I = 0.1$ M)	$\log(K^{\circ}_{S,0})$ ($\theta = 25°C$, $I = 0.1$ M)
#1	8.9×10^{-3}	5.9×10^{-3}	2.4×10^{-3}	2.1×10^{-21}	−45.5	$-(53.7 \pm 0.4)$
#2	1.4×10^{-3}	2.0×10^{-2}	1.1×10^{-4}	2.7×10^{-20}	−46.9	$-(55.5 \pm 0.7)$
#3	1.3×10^{-3}	2.0×10^{-2}	1.1×10^{-4}	2.7×10^{-20}	−46.8	$-(55.5 \pm 0.7)$
#4	1.4×10^{-3}	6.6×10^{-2}	1.9×10^{-5}	9.4×10^{-20}	−45.8	$-(56.7 \pm 0.7)$
#5	2.0×10^{-3}	5.4×10^{-2}	2.0×10^{-5}	8.2×10^{-19}	−43.7	$-(54.7 \pm 0.7)$
#6	7.4×10^{-3}	2.0×10^{-1}	6.4×10^{-6}	3.9×10^{-18}	−43.8	$-(54.8 \pm 0.7)$
Average value						$-(\mathbf{55.1 \pm 0.9})$
Sandino [59]						$-(53.3 \pm 0.3)$
Schreyer [60]						$-(49.6 \pm 0.5)$
Pekarek [49]						$-(49.4 \pm 0.5)$
Karpov [59]						$-(48.8 \pm 0.5)$

[a] Calculated from under saturation (sample #1) and over-saturation (samples #5 and #6) experiments on $(UO_2)_3(PO_4)_2 \cdot 5H_2O$ or from leaching tests of $U(UO_2)(PO_4)_2$ (sample #2), $U_2O(PO_4)_2$ (sample #3) or α-UP_2O_7 (sample #4).

$$\log(\gamma_{PO_4^{3-}}) = -(z_{PO_4^{3-}})^2 D + \varepsilon_{(PO_4^{3-},X)} m_X, \tag{14}$$

and

$$D = \frac{A\sqrt{I_m}}{1 + Ba_j\sqrt{I_m}}, \tag{15}$$

where I_m is the ionic strength (in mol kg^{-1}). In this expression, A and B are temperature and pressure dependent constants while a_j is an ion size parameter 'distance of closest approach' for the hydrated ion j. For these calculations, the A and $B \times a_j$ values were taken to 0.509 and 1.5 $kg^{1/2}$ $mol^{-1/2}$, respectively, as proposed by Ciavatta et al. [56]. The water activity was calculated considering the recommendation given by Silva et al. [57]. Moreover, we considered the following specific interaction coefficient values: $\varepsilon(UO_2^{2+}, NO_3^-) = 0.24 \pm 0.03$ and $\varepsilon(PO_4^{3-}, Na^+) = 0.25 \pm 0.03$. The contribution of all the minor species were neglected. The concentrations of the free uranyl $[UO_2^{2+}]$ and phosphate $[PO_4^{3-}]$ ions were calculated using the CHESS program [58].

The results obtained during the first and second ways of determination, on one hand, and the third way, on the other hand, are reported in Tables 10 and 11, respectively. These values are in good agreement with those reported by several authors [49,59–61] (Table 10). The slight discrepancies observed between the results could be due to the formation of $(UO_2)_3(PO_4)_2 \cdot 5H_2O$ with different crystallinity. Furthermore, additional discrepancies could be due to the $\varepsilon(i,j)$ set used to extrapolate the solubility product for an ionic strength equal to 0 [62].

In order to confirm that the formation of $(UO_2)_3(PO_4)_2 \cdot 5H_2O$ is controlled by a thermodynamic equilibrium, its synthesis was performed using oversaturation experiments. Several samples of powdered uranyl phosphate pentahydrate were precipitated at 90°C from a mixture of phosphoric acid and uranyl nitrate solution considering several initial conditions then characterized. Several ratios were considered with different concentrations of uranium and phosphate. After a few days of contact, XRD and EPMA analyses of the precipitates obtained indicate the precipitation of $(UO_2)_3(PO_4)_2 \cdot 5H_2O$ for initial mole ratios U/PO_4 in the solution near to 3/2. For mole ratios lower, the

Table 11
Solubility product, $K^{\circ}_{S,0}$, of $(UO_2)_3(PO_4)_2 \cdot 5H_2O$ calculated from the leaching tests performed on TUPD solid solutions

Sample[a]	$C_{UO_2^{2+}}$ (M)	$C_{PO_4^{3-}}$ (M)	$[UO_2^{2+}]$ (M)	$[PO_4^{3-}]$ (M)	$\log([UO_2^{2+}]^3[PO_4^{3-}]^2)$ ($\theta = 90°C$, $I = 0.1$ M)	$\log(K^{\circ}_{S,0})$ ($\theta = 25°C$, $I = 0.1$ M)
#7	3.3×10^{-3}	6.9×10^{-2}	4.5×10^{-5}	9.5×10^{-20}	−44.6	$-(55.5 \pm 0.7)$
#8	7.2×10^{-4}	3.2×10^{-2}	6.2×10^{-6}	2.6×10^{-18}	−43.9	$-(55.3 \pm 0.3)$
#9	7.5×10^{-4}	3.5×10^{-2}	5.4×10^{-6}	2.9×10^{-18}	−43.7	$-(55.3 \pm 0.3)$
#10	8.8×10^{-4}	3.8×10^{-2}	5.6×10^{-6}	3.1×10^{-18}	−43.5	$-(55.2 \pm 0.3)$
Average value						$-(\mathbf{55.3 \pm 0.1})$

[a] Calculated from leaching tests of TUPD in 10^{-1} M HNO_3 (sample #7), 10^{-2} M HNO_3 (sample #8), 10^{-3} M HNO_3 (sample #9) or 10^{-4} M HNO_3 (sample #10) at 90°C considering the precipitation of the thorium phosphate–hydrogenphosphate hydrate $Th_2(PO_4)_2(HPO_4) \cdot H_2O$ which solubility product $K^{\circ}_{S,0}$ was evaluated to $10^{-66.6 \pm 1.2}$ [33].

precipitation of $UO_2HPO_4 \cdot 4H_2O$ was simultaneously observed. Many authors also mentioned the precipitation of the uranyl phosphate hexahydrate but we did not observe this compound probably because of the temperature of experiments ($\theta = 90°C$). That is coherent with the results reported by Karpov and Kobets in which the authors reported the formation of the $(UO_2)_3(PO_4)_2 \cdot 6H_2O$ for temperatures lower than 40°C [63,64]. Furthermore, from Schreyer et al. [60], $UO_2HPO_4 \cdot 4H_2O$ precipitates for a total phosphate concentration in the range 1.4×10^{-2} M–6.1 M which corresponds to the range of concentration we measured. Nevertheless, we did not observe the formation of such a solid in our experiments.

5. Conclusion

The thorium phosphate–diphosphate appears as a good candidate for the immobilization of tetravalent uranium. Indeed, it allows the substitution of large amounts of thorium by uranium (IV) and it is easy to prepare whatever the chemical ways of synthesis. Moreover, this matrix is very resistant to aqueous corrosion. As observed for TPD, the dissolution of TUPD involves two successive steps. The first one is kinetically-controlled while the second one corresponds to a thermodynamic equilibrium.

In the first part of the dissolution curves obtained, a linear increase of the uranium content is observed. For all the media studied, the normalized dissolution rates remain small even in very corrosive medium. Several parameters like temperature, pH and background salt were studied. From the preliminary results, the apparent activation energy of the dissolution reaction of TUPD was evaluated to 40 kJ mol^{-1} which is characteristic of mechanism controlled by surface reactions. The variation of the normalized dissolution rate with the pH gave a partial order related to the proton equal to 0.40 ± 0.02 while the apparent normalized dissolution rate constant was found to 3.10^{-4} g m^{-2} d^{-1} at 90°C. These values are in good agreement with those obtained for the pure TPD at 25°C or for samples doped with small amounts of trivalent actinides. The background salt influence study showed that the presence of perchlorate ions instead of nitrate ions leads to dissolution rates smaller than those obtained in nitric acid because of the slower oxidization of tetravalent uranium into uranyl.

The second step controlling the dissolution of TUPD solid solutions corresponds to the formation of neoformed phases. It was observed for leaching time exceeding 60 days in 10^{-1} M HNO_3 or for 150 days in 10^{-2}–10^{-4} M HNO_3. In the leachate, the uranium and thorium concentrations are controlled by the precipitation of the uranyl phosphate pentahydrate $(UO_2)_3(PO_4)_2 \cdot 5H_2O$ and the thorium phosphate–hydrogenphosphate $Th_2(PO_4)_2HPO_4 \cdot H_2O$, respectively. These solids were extensively characterized. They are very low-soluble which allows one to propose the TPD as a promising matrix for the actinides immobilization and especially for uranium, neptunium and plutonium. Indeed, the kinetic of the TPD dissolution is very slow, leading to good retention properties regarding to the actinides studied. Moreover, as the neoformed phases are very low-soluble, the migration of actinides will be delayed by their precipitation as phosphate phases.

The chemical behavior of sintered TUPD samples is now under study. The preliminary dissolution rates calculated (6.5×10^{-5} g d^{-1}) are lower than that reported for powdered samples (5.4×10^{-4} g d^{-1}) due to the significant decrease of the effective surface in contact with the solution during leaching tests compared to the powdered samples.

References

[1] J. Carpena, F. Audubert, D. Bernache, L. Boyer, B. Donazzon, J.L. Lacout, N. Senamaud, Mater. Res. Soc. Proc. 506 (1998) 543.
[2] L.A. Boatner, B.C. Sales, in: W. Lutze and R.C. Ewing (Eds.), Radioactive Waste Forms for the Future, North-Holland Physics, Amsterdam, 1998, p. 495.
[3] H.T. Hawkins, B.E. Scheetz, G.D. Guthrie Jr., Mater. Res. Soc. Symp. Proc. 465 (1996) 387.
[4] V. Brandel, N. Dacheux, M. Genet, J. Solid State Chem. 121 (1996) 467.
[5] P. Benard, V. Brandel, N. Dacheux, S. Jaulmes, S. Launay, C. Lindecker, M. Genet, D. Louër, M. Quarton, Chem. Mater. 8 (1996) 181.
[6] V. Brandel, N. Dacheux, M. Genet, Radiokhimiya 43 (2001) 16.
[7] A.C. Thomas, N. Dacheux, V. Brandel, P. Le Coustumer, M. Genet, J. Nucl. Mater. 281 (2000) 91.
[8] N. Dacheux, A.C. Thomas, B. Chassigneux, V. Brandel, M. Genet, in: J.C. Marra, G.T. Chandler (Eds.), Environmental Issues and Waste Management Technologies in Ceramics and Nuclear Industries IV, vol. 93, 1999, p. 373.
[9] N. Dacheux, R. Podor, B. Chassigneux, V. Brandel, M. Genet, J. Alloys Comp. 271 (1998) 236.
[10] N. Dacheux, R. Podor, V. Brandel, M. Genet, J. Nucl. Mater. 252 (1998) 179.
[11] N. Dacheux, V. Brandel, M. Genet, K. Bak, C. Berthier, New J. Chem. 20 (1996) 301.
[12] N. Dacheux, A.C. Thomas, P. Le Coustumer, V. Brandel, M. Genet, J. Nucl. Mater. 257 (1998) 108.
[13] N. Dacheux, V. Brandel, M. Genet, P. Le Coustumer, R. Podor, to be published.
[14] A.C. Thomas, N. Dacheux, P. Le Coustumer, V. Brandel, M. Genet in: D.R. Spearing, (Ed.), Environmental and Waste Management Technologies in the Ceramic and Nuclear Industries VI, vol. 119, 2001.
[15] M. Evain, U-Fit Program, Institut des Matériaux de Nantes, France, 1992.

[16] A. Oberlin, in: P.A. Thrown, M. Dekker (Eds.), Chemistry and Physics of Carbon, vol. 22, Marcel Dekker, New York, 1989, p. 1.
[17] J.N. Rouzaud, A. Oberlin, M. Vandenbroucke, C.R. Somm, Soc. Géol. Fr. 5 (1978) 238.
[18] N. Dacheux, J. Aupiais, Anal. Chem. 69 (1997) 2275.
[19] A.C. Lasaga, in: A.F. White, S.L. Brantley (Eds.), Rev. Mineral., 31 (1995) 23.
[20] G.R. Holdren Jr., R.A. Berner, Geochim. Cosmochim. Acta 43 (1979) 1161.
[21] R.A. Berner, E.L. Sjoberg, M.A. Vebel, M.D. Krom, Science 207 (1980) 1205.
[22] R. Petrovic, Geochim. Cosmochim. Acta 40 (1976) 1509.
[23] W. Stumm, G. Furrer, B. Kunz, Croat. Chem. Acta 56 (1983) 593.
[24] A.C. Lasaga, J. Geophys. Res. 89 (1984) 4009.
[25] A.C. Lasaga, in: A.C. Lasaga, R.J. Kirkpatrick (Eds.), Kinetics of Geochemical Processes, Rev. Mineral. 8 (1981) 1.
[26] L. Chou, R. Wollast, Am. J. Sci. 285 (1985) 963.
[27] G. Furrer, W. Stumm, Geochim. Cosmochim. Acta 50 (1986) 1847.
[28] H.C. Hegelson, W.M. Murphy, P. Aagaard, Geochim. Cosmochim. Acta 78 (1984) 2405.
[29] A.E. Blum, A.C. Lasaga, Nature 331 (1988) 431.
[30] L. Chou, R. Wollast, J.I. Drever (Ed.), The Chemistry of Weathering, Reidel, Dordrecht, 1985, p. 75.
[31] J. Schott, R.A. Berner, E.L. Sjoberg, Geochim. Cosmochim. Acta 45 (1981) 2123.
[32] V.N. Fleer, PhD thesis, Pennsylvania State University, University Park, PA, 1982.
[33] A.C. Thomas, N. Dacheux, J. Aupiais, V. Brandel, M. Genet, to be published.
[34] N.M. Rose, Geochim. Cosmochim. Acta 55 (1991) 3273.
[35] S.A. Caroll, PhD thesis, Northwestern University, Evanston, 1989.
[36] S.A. Caroll-Webb, J.V. Walther, Am. J. Sci. 290 (1998) 797.
[37] P.S. Schweda, in: E. Miles (Ed.), Water–Rock Interaction, Balkema, Rotterdam, 1989, p. 609.
[38] W.H. Casey, M.F. Hochella, H.R. Westrich, Geochim. Cosmochim. Acta 57 (1993) 785.
[39] N. Dacheux, A.C. Thomas, B. Chassigneux, E. Pichot, V. Brandel, M. Genet, Mater. Res. Soc. Proc. 556 (1999) 85.
[40] N. Dacheux, A.C. Thomas, B. Chassigneux, V. Brandel, M. Genet, in: G.T. Chandler, X. Feng (Eds.), Environmental and Waste Management Technologies in the Ceramic and Nuclear Industries V, vol. 107, 2000, p. 333.
[41] M. Genet, N. Dacheux, A.C. Thomas, B. Chassigneux, E. Pichot, V. Brandel, in: WM'99 Conference Proceedings, 1999.
[42] N. Dacheux, V. Brandel, M. Genet, New J. Chem. 19 (1995) 15.
[43] N. Dacheux, V. Brandel, M. Genet, New J. Chem. 19 (1995) 1029.
[44] P. Bernard, D. Loüer, N. Dacheux, V. Brandel, M. Genet, Anal. Quim. Int. Ed. 92 (1996) 79.
[45] M. Saadi, C. Dion, F. Abraham, J. Solid State Chem. 150 (2000) 72.
[46] V. Brandel, N. Dacheux, M. Genet, R. Podor, J. Solid State Chem. (2001) in press.
[47] J.R. Ferraro, A. Walker, J. Chem. Phys. 45 (1966) 550.
[48] H. Gerding, G. Prins, W. Gabes, Rev. Chim. Mineral. 12 (1975) 303.
[49] V. Pekarek, V. Vesely, J. Inorg. Nucl. Chem. 27 (1965) 1157.
[50] N. Dacheux, thesis, University of Paris-Sud, IPNO-T-95.04, 1995.
[51] M. Knidiri, Thesis, University of Paris VI, A.O.10.552, 1974.
[52] S.P. Mc Glynn, J.K. Smith, W.C. Neely, J. Chem. Phys. 35 (1961) 105.
[53] J.R. Bartlett, R.P. Cooney, J. Molec. Struct. 193 (1989) 295.
[54] R.G. Denning, Gmelin Handbuch Anorg. Chem. A 6 (1983) 55.
[55] P. Le Coustumer, M. Monthioux, A. Oberlin, Br. Ceram. Trans. 5 (1995) 177.
[56] L. Ciavatta, Ann. Chim. (Roma) 70 (1980) 551.
[57] R.J. Silva, G. Bidoglio, M.H. Rand, P.B. Robouch, H. Wanner, I. Puigdomenech, in: Chemical Thermodynamics of Americium, OECD, Elsevier, Amsterdam, 1995.
[58] J. Van der Lee, L. de Windt, Technical report LHM/RD/99/05, Ecole des Mines de Paris, Fontainebleau, France, 1999.
[59] A. Sandino, J. Bruno, Geochim. Cosmochim. Acta 56 (1992) 4135.
[60] J.M. Schreyer, C.F. Baes, J. Am. Chem. Soc. 76 (1954) 354.
[61] V.I. Karpov, Russ. J. Inorg. Chem. 6 (1961) 271.
[62] I. Grenthe, J. Fuger, R.J.M. Konings, R.J. Lemire, A.B. Muller, C. Nguyen-Trung, H. Wanner, in: H. Wanner, I. Forest (Eds.), Chemical Thermodynamics of Uranium, Elsevier, Amsterdam, 1992, p. 715.
[63] V.I. Karpov, T.L. Ambartsumya, Russ. J. Inorg. Chem. 7 (1962) 949.
[64] L.V. Kobets, T.A. Kolevich, D.S. Umreiko, Russ. J. Inorg. Chem. 23 (1978) 501.